Joint-Track Equalization and Detection for Bit Patterned Media Recording

Seyhan Karakulak, Paul H. Siegel, *Fellow, IEEE*, Jack Keil Wolf, *Life Fellow, IEEE*, and H. Neal Bertram, *Life Fellow, IEEE*

Center for Magnetic Recording Research, University of California, San Diego, La Jolla, CA 92093-0401 USA

We compare several different detection and equalization methods for bit patterned media recording channels. We consider a scheme that utilizes a joint-track equalization technique followed by a Viterbi detector. For certain recording densities, simulation results show that it has essentially the same performance as an optimal detector but with reduced detection complexity. Furthermore, it outperforms another scheme of the same complexity previously described in the literature.

***Index Terms*—Bit patterned media (BPM) recording, joint-track equalization, maximum *a posteriori* (MAP) detection, maximum-likelihood (ML) detection.**

I. Introduction

THE superparamagnetic effect poses an obstacle to increasing the areal density in perpendicular recording. Bit patterned media (BPM) recording is one method being proposed to circumvent the density limitations imposed by this effect [1]. In BPM, magnetic bits are recorded on pre-defined, single-domain "islands."

It is conceivable that early generations of BPM will utilize read heads whose dimensions are larger than an island of magnetization. For such a scenario, we introduced a technique to compute the output of BPM recording channels [2]. This technique allows the signal contribution due to the inter-track interference (ITI) from adjacent tracks to be evaluated.

In this paper, the read head centered over the main track spans a specified fraction of the outer tracks (*upper track* and *lower track*, respectively). This is shown schematically in Fig. 1. If binary data is recorded on each track, the triplet of islands represents one of 8 possible recorded "symbols." That is, each symbol represents three independent bits stored on the upper, main, and lower track.

Several detection and equalization methods have been proposed for channels with ITI. The performance of the read channel in the presence of additive white Gaussian noise (AWGN) was analyzed under maximum-likelihood (ML) symbol sequence detection in [2]. The complexity of an ML detector for the bit sequence written on the main track is substantial in the presence of ITI. In [3], a detector that utilizes ML symbol sequence detection and outputs the middle bit of each detected symbol in the ML symbol sequence was introduced. To reduce the detection complexity, in [4], a decision feedback equalizer (DFE) that uses the previously detected upper track data was proposed. In [5], ML symbol sequence detection with joint-track equalization was described. A maximum *a posteriori* (MAP) bit detector was derived in [6]. In [7], a one-dimensional (1-D) equalizer was designed where a partial-response (PR) target was chosen to match the channel response of the main track. For detection, the Viterbi algorithm was utilized on a modified trellis where the number of states corresponded to the PR target. The modified trellis was obtained by adding branches to take into account the ITI from immediately adjacent bits on the outer tracks.

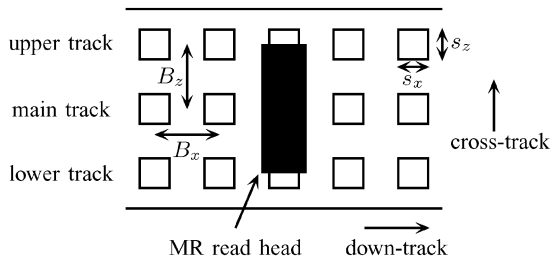

Fig. 1. Schematic of the magnetoresistive head and patterned magnetic medium.

In [8] and [9], a two-dimensional (2-D) generalized partial-response (GPR) equalizer that eliminates the ITI followed by a Viterbi detector was introduced. In [9], the use of iterative decision feedback detection (IDFD) was proposed. For IDFD or 2-D equalization, multiple 1-D waveforms were required as inputs rather than a single 1-D waveform as in the methods described above. These multiple 1-D waveforms might be obtained by reading multiple adjacent tracks or by utilizing multi-head read elements.

In this work, we consider the detection of the bit sequence written on the main track only. In Section II, we first review the read channel model described in [2]. Later, we discuss head and media configurations for different recording densities. In Section III, we study ML bit sequence detection and MAP bit detection. In Section IV, we review briefly several previously designed 1-D and 2-D equalizers. We adapt a joint-track equalizer introduced in [5] to BPM recording channels. In Section V, we propose a scheme that utilizes the joint-track equalizer followed by a Viterbi detector. We compare the performance and the complexity of this scheme with schemes that utilize optimal bit detection or optimal symbol sequence detection, and the scheme introduced in [7]. The latter scheme consists of 1-D equalization with a PR target followed by the Viterbi algorithm that works on the modified trellis as described above. We have also considered the scheme introduced in [7] with optimized 1-D equalizer/target coefficients.

Manuscript received October 08, 2008; revised January 09, 2009, May 28, 2009, and March 19, 2010; accepted April 19, 2010. Date of publication May 03, 2010; date of current version August 20, 2010. Corresponding author: S. Karakulak (e-mail: skarakul@ucsd.edu).

Color versions of one or more of the figures in this paper are available online at http://ieeexplore.ieee.org.

Digital Object Identifier 10.1109/TMAG.2010.2049116

TABLE I
MEDIA CONFIGURATIONS

Recording density	s_x	s_z	B_x	B_z
1 Tb/in^2	12.5 nm	12.5 nm	25 nm	25 nm
1.2 Tb/in^2	11 nm	12.5 nm	21.5 nm	25 nm
1.4 Tb/in^2	9 nm	12.5 nm	18.4 nm	25 nm
1.75 Tb/in^2	7 nm	12.5 nm	14.7 nm	25 nm
2 Tb/in^2	6 nm	12.5 nm	12.9 nm	25 nm

II. READ CHANNEL MODEL

In the read channel model [2], the islands are arranged on a rectangular grid with each island representing a single bit as shown in Fig. 1. In the figure, s_x and s_z represent the dimensions of the islands in the down-track and cross-track directions, respectively. Center to center island distance is denoted by B_x in the down-track direction whereas it is denoted by B_z in the cross-track direction.

Reading is accomplished with a finite track-width magnetoresistive (MR) head with infinitely wide shields. The head potential distribution is obtained using reciprocity calculations and is modified for the presence of a soft underlayer (SUL) using the method of multiple images [10], [11]. The contribution of a magnetized island to the readback signal is evaluated as the integral of the head potential distribution over that island.

The readback signal is passed through a low-pass filter, followed by a sampler with a sampling interval corresponding to the down-track island separation. Electronics noise, modeled as AWGN, is assumed to corrupt the output of the read head.

We consider recording densities between 1 Tb/in^2 and 2 Tb/in^2. The same read head of width 40 nm, with a gap width 20 nm, and MR element thickness 7 nm is utilized for different recording densities. Table I shows media configurations for the recording densities considered in this study. Note that the parameter B_z which determines the track period is set to 25 nm whereas the parameter B_x is scaled down to obtain higher recording densities. By setting the parameter B_z to a fixed value, we obtain a relatively constant amount of ITI for different recording densities. For certain recording densities, the noiseless sampled discrete-time readback model can be represented by a 3×3 channel response matrix H

$$H = \begin{pmatrix} h_{0,-1} & h_{1,-1} & h_{2,-1} \\ h_{0,0} & h_{1,0} & h_{2,0} \\ h_{0,1} & h_{1,1} & h_{2,1} \end{pmatrix}. \tag{1}$$

Here, the inter-symbol interference (ISI) is limited to 2 symbols. Each entry in the channel response matrix H represents the relative contribution of each island that the head senses. Let

$$h_{-1}(D) = \sum_{k=0}^{2} h_{k,-1} D^k \tag{2}$$

$$h_0(D) = \sum_{k=0}^{2} h_{k,0} D^k \tag{3}$$

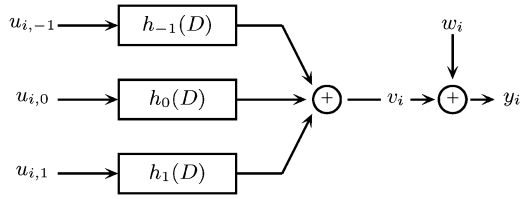

Fig. 2. Read channel model.

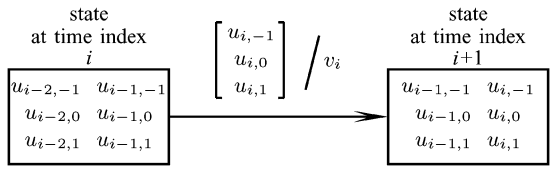

Fig. 3. State and branch labeling for the channel response matrix H.

and

$$h_1(D) = \sum_{k=0}^{2} h_{k,1} D^k \tag{4}$$

where D denotes the delay operator. Then, $h_{-1}(D)$, $h_0(D)$, and $h_1(D)$ represent the channel transfer polynomials of the upper, main, and lower tracks, respectively. A schematic of the sampled read channel model is shown in Fig. 2. The channel inputs are assumed to be independent, identically distributed (i.i.d.), equiprobable binary sequences $\{u_{i,-1}\}$, $\{u_{i,0}\}$, and $\{u_{i,1}\}$, where $u_{i,-1}, u_{i,0}, u_{i,1} \in \{1, -1\}$. The noise samples $\{w_i\}$ are assumed to be independent, zero-mean Gaussian random variables with variance σ^2. Then, the readback signal y_i at time index i is

$$\begin{aligned} y_i &= \sum_{k=0}^{2} h_{k,-1} u_{i-k,-1} + \sum_{k=0}^{2} h_{k,0} u_{i-k,0} + \sum_{k=0}^{2} h_{k,1} u_{i-k,1} + w_i \\ &\triangleq v_i + w_i \end{aligned} \tag{5}$$

where v_i is the noiseless output signal.

The channel given in (1) has a memory of two symbols where each symbol takes on eight values. The input and noiseless output sequences of this channel can then be described by a trellis with $8^2 = 64$ states and eight outgoing branches from each state to eight follower states. Each state at time index i is labeled with the symbols at time indices $i-2$ and $i-1$, respectively. From each state at time index i, there are eight outgoing branches to eight different states at time index $i+1$. The branches emanating from the state at time index i are labeled by the input symbol at time index i and the noiseless output v_i corresponding to this state transition. This is shown in Fig. 3.

For the case where the channel has cross-track symmetry, that is, when $h_{0,-1} = h_{0,1}$, $h_{1,-1} = h_{1,1}$, and $h_{2,-1} = h_{2,1}$, the input and noiseless output sequences can be represented with a trellis that has $6^2 = 36$ states. For convenience, we define a

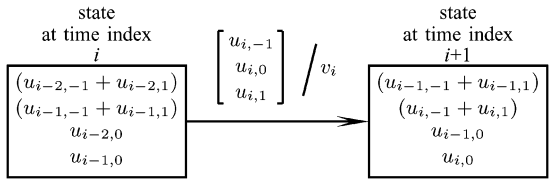

Fig. 4. State and branch labeling for the channel response matrix H with a cross-track symmetry.

channel response matrix H_c with this cross-track symmetry as follows:

$$H_c = \begin{pmatrix} m & p & n \\ r & q & t \\ m & p & n \end{pmatrix}. \tag{6}$$

Each state at time index i is labeled with four quantities: the sum of the bits on the upper and lower tracks at time index $i-2$, the sum of the bits on the upper and lower tracks at time index $i-1$, the bit on the main track at time index $i-2$, and the bit on the main track at time index $i-1$. Each branch is labeled in a manner similar to the case of channel response H in (1). This is shown in Fig. 4. The sum of the bits written on the upper and lower tracks at time index i takes three different values as follows:

$$(u_{i,-1}+u_{i,1}) = \begin{cases} -2, & \text{if } u_{i,-1}=-1 \text{ and } u_{i,1}=-1 \\ 0, & \text{if } u_{i,-1}=-1 \text{ and } u_{i,1}=1 \\ 0, & \text{if } u_{i,-1}=1 \text{ and } u_{i,1}=-1 \\ +2, & \text{if } u_{i,-1}=1 \text{ and } u_{i,1}=1. \end{cases} \tag{7}$$

Therefore, the trellis representing the channel input and noiseless channel output sequences has $(3\times 3\times 2\times 2)=6^2=36$ different states. If we denote the noiseless channel outputs at time index i for the input $\{u_{i,-1}=1, u_{i,1}=-1\}$ by $v_i^{(1)}$ and for the input $\{u_{i,-1}=-1, u_{i,1}=1\}$ by $v_i^{(2)}$, we find that

$$\begin{aligned} v_i^{(1)} &= n(u_{i-2,-1}+u_{i-2,1}) + p(u_{i-1,-1}+u_{i-1,1}) + m(0) \\ &\quad + t(u_{i-2,0}) + q(u_{i-1,0}) + r(u_{i,0}) \end{aligned} \tag{8}$$

$$\begin{aligned} v_i^{(2)} &= n(u_{i-2,-1}+u_{i-2,1}) + p(u_{i-1,-1}+u_{i-1,1}) + m(0) \\ &\quad + t(u_{i-2,0}) + q(u_{i-1,0}) + r(u_{i,0}). \end{aligned} \tag{9}$$

It is seen from (8) and (9) that $v_i^{(1)}$ and $v_i^{(2)}$ are equal. There are two such pairs of inputs for which the noiseless channel outputs are the same, i.e., one pair when $u_{i,0}=-1$ and one pair when $u_{i,0}=1$. Therefore, in this trellis structure, more than one input symbol sequence may generate the same noiseless output sequence. When using this trellis as the basis for symbol detection, we may have to use a restricted input symbol alphabet [2]. Alternatively, we may use the reduced-state trellis for only detection of the bit sequence recorded on the main track.

In addition to the cross-track symmetry, if the corner entries $h_{0,-1}$, $h_{0,1}$, $h_{2,-1}$, and $h_{2,1}$ are equal to zero, the input and the noiseless output sequences can be represented with a 4-state trellis [7]. For convenience, we define a channel response matrix H_+ having the cross-track symmetry and with the corner entries equal to zero as follows:

$$H_+ = \begin{pmatrix} 0 & p & 0 \\ r & q & t \\ 0 & p & 0 \end{pmatrix}. \tag{10}$$

Details of the trellis for this channel and detectors for pending the input sequence on the main track are described in the next section.

III. Detection

In this section, we study ML bit sequence detection and MAP bit detection for the sequence written on the main track, $\underline{u}_0$.

A. ML Bit Sequence Detection

The ML bit sequence detected from the main track is the sequence $\hat{\underline{u}}_0$ that maximizes $p(\underline{y}|\underline{u}_0)$, i.e.,

$$\begin{aligned} \hat{\underline{u}}_0 &= \arg\max_{\underline{u}_0} p(\underline{y}|\underline{u}_0) \\ &= \arg\max_{\underline{u}_0} \left[\sum_{\underline{u}_{-1}} \sum_{\underline{u}_1} p(\underline{y}, \underline{u}_{-1}, \underline{u}_1 | \underline{u}_0) \right] \\ &= \arg\max_{\underline{u}_0} \left[\sum_{\underline{u}_{-1}} \sum_{\underline{u}_1} p(\underline{y}|\underline{u}_0, \underline{u}_{-1}, \underline{u}_1) P(\underline{u}_{-1}, \underline{u}_1) \right] \end{aligned} \tag{11}$$

where $\underline{y}$ represents the detector input samples and $P(\underline{u}_{-1}, \underline{u}_1)$ represents the joint *a priori* probability of the bit sequences $\underline{u}_{-1}$ and $\underline{u}_1$. Since the sequences $\underline{u}_{-1}$ and $\underline{u}_1$ are i.i.d. equiprobable,

$$\hat{\underline{u}}_0 = \arg\max_{\underline{u}_0} \left[\sum_{\underline{u}_{-1}} \sum_{\underline{u}_1} p(\underline{y}|\underline{u}_0, \underline{u}_{-1}, \underline{u}_1) \right]. \tag{12}$$

The complexity involved in the maximization of $p(\underline{y}|\underline{u}_0)$ is proportional to the number of distinct pairs $(\underline{u}_{-1}, \underline{u}_1)$. Therefore, it is substantial. As stated in [5], if at a high signal-to-noise ratio (SNR), the conditional densities involved in (12) are dominated by one particular pair $(\underline{u}_{-1}, \underline{u}_1)$, the following approximation can be made:

$$\max_{\underline{u}_0} \left[\sum_{\underline{u}_{-1}} \sum_{\underline{u}_1} p(\underline{y}|\underline{u}_0, \underline{u}_{-1}, \underline{u}_1) \right] \approx \max_{\underline{u}_0, \underline{u}_{-1}, \underline{u}_1} p(\underline{y}|\underline{u}_0, \underline{u}_{-1}, \underline{u}_1). \tag{13}$$

The right-hand side of (13) corresponds to joint ML sequence detection for $\underline{u}_{-1}$, $\underline{u}_0$, and $\underline{u}_1$, i.e., ML symbol sequence detection. Thus, a detection scheme, based on the Viterbi algorithm, that outputs the middle bit of each detected symbol in the ML symbol sequence can be viewed as a high SNR approximation for ML bit sequence detection. For channels with a cross-track symmetry, ML symbol sequence detector works on the 36-state trellis described in the previous section.

When the channel response matrix is equal to H_+ as defined in (10), the ML bit sequence can be obtained using the Viterbi

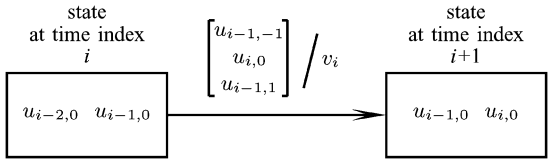

Fig. 5. State and branch labeling for the channel response matrix H_+.

algorithm with a modified branch metric on a 4-state trellis with four parallel branches between each connected pair of states. Each branch is labeled by the channel input bit on the upper track at time index $i-1$, the channel input bit on the main track at time index i, the channel input bit on the lower track at time index $i-1$, and the noiseless channel output v_i. This is shown in Fig. 5. We represent each state at time index i with s_i, where

$$s_i \stackrel{\text{def}}{=} (u_{i-2,0}, u_{i-1,0}). \tag{14}$$

Let K denote the length of the input bit sequence $\underline{u}_0$. We assume that the initial and final states s_0 and s_K are known. There is a one-to-one correspondence between state sequences $\underline{s} = \{s_0, s_1, \ldots, s_K\}$ and input bit sequences $\underline{u}_0 = \{u_{0,0}, u_{1,0}, \ldots, u_{K-1,0}\}$ written on the main track. Therefore, the ML bit sequence detector finds the state sequence $\hat{\underline{s}}$ that maximizes $p(\underline{y}|\underline{s})$, i.e.,

$$\begin{aligned}\hat{\underline{s}} &= \arg\max_{\underline{s}} p(\underline{y}|\underline{s}) \\ &= \arg\max_{\underline{s}} \prod_{i=0}^{K-1} p(y_i|s_i, s_{i+1}).\end{aligned} \tag{15}$$

Define

$$\lambda(s_i, s_{i+1}) \stackrel{\text{def}}{=} -\ln p(y_i|s_i, s_{i+1}). \tag{16}$$

Maximizing $p(\underline{y}|\underline{s})$ is the same as minimizing $-\ln p(\underline{y}|\underline{s})$ and the latter can be expressed as

$$-\ln p(\underline{y}|\underline{s}) = \sum_{i=0}^{K-1} \lambda(s_i, s_{i+1}). \tag{17}$$

The detector can be implemented using the Viterbi algorithm with a modified branch metric equal to $\lambda(s_i, s_{i+1})$. We can express $\lambda(s_i, s_{i+1})$ as follows:

$$\begin{aligned}\lambda(s_i, s_{i+1}) &= -\ln p(y_i|s_i, s_{i+1}) \\ &= -\ln\left[\sum_{u_{i-1,-1}}\sum_{u_{i-1,1}} p(y_i, u_{i-1,-1}, u_{i-1,1}|s_i, s_{i+1})\right] \\ &= -\ln\big[p(y_i|s_i, s_{i+1}, u_{i-1,-1}=-1, u_{i-1,1}=-1) \\ &\qquad \times P(u_{i-1,-1}=-1, u_{i-1,1}=-1) \\ &\qquad + p(y_i|s_i, s_{i+1}, u_{i-1,-1}=-1, u_{i-1,1}=1) \\ &\qquad \times P(u_{i-1,-1}=-1, u_{i-1,1}=1) \\ &\qquad + p(y_i|s_i, s_{i+1}, u_{i-1,-1}=1, u_{i-1,1}=-1) \\ &\qquad \times P(u_{i-1,-1}=1, u_{i-1,1}=-1) \\ &\qquad + p(y_i|s_i, s_{i+1}, u_{i-1,-1}=1, u_{i-1,1}=1) \\ &\qquad \times P(u_{i-1,-1}=1, u_{i-1,1}=1)\big].\end{aligned} \tag{18}$$

The detection algorithm based upon (18) can be thought of in terms of the Viterbi algorithm operating on a 4-state trellis where a single branch replaces the four parallel branches between connected states. The branch metric for this single branch is given by (18). This detector is an ML detector for the bit sequence written on the main track.

Another detector which operates on a 4-state trellis which has three parallel branches between connected states was described in [7]. As stated in [7], that detector first finds the best branch out of the parallel branches between connected states. The two detectors are not the same in that there are situations where for a given noisy output sequence they will choose different input sequences. Since our detector is an ML detector, it follows that the detector described in [7] is not truly an ML detector.

B. MAP Bit Detection

The Bahl-Cocke-Jelinek-Raviv (BCJR) algorithm outputs the *a posteriori* probability (APP) for each symbol given the detector input samples. Here, we present only a brief review of the BCJR algorithm and highlight the modification needed to obtain the APP for the bit written on the main track corresponding to -1 and 1. This modification was derived in [6]. A detailed description of the BCJR algorithm can be found in [12].

The BCJR algorithm operates on the trellis representing the noiseless channel output sequences. It recursively computes the *forward state metrics* and the *backward state metrics*, which are combined with the *branch metrics* to produce the APP of each symbol.

If $u_{i,0}$ represents a recorded bit on the main track at time index i and $\underline{y}$ represents the detector input samples, the modified BCJR algorithm outputs

$$P[u_{i,0} = -1|\underline{y}] = \sum_{U_i^{-1}} P[u_{i,-1}, u_{i,0}, u_{i,1}|\underline{y}] \tag{19}$$

$$P[u_{i,0} = 1|\underline{y}] = \sum_{U_i^{1}} P[u_{i,-1}, u_{i,0}, u_{i,1}|\underline{y}]. \tag{20}$$

Here, U_i^{-1} and U_i^1 are the set of symbols at time index i, where $u_{i,0}$ equals -1 and 1, respectively. Note that when the channel response has a cross-track symmetry, the 36-state trellis described in Section II can also be utilized for MAP bit detection.

IV. Equalization

In this section, we review several previously designed equalizers for BPM recording channels. We later adapt the use of a joint-track equalizer introduced in [5] in the context of single-head/single-track detection for perpendicular recording channels to BPM recording channels.

A. Related Equalization Techniques

In [13], 1-D *minimum mean-square error* (MMSE) finite impulse response (FIR) equalizers were discussed for BPM recording channels. A block diagram of this 1-D equalization, where the ITI was treated as noise, is shown in Fig. 6. The channel response can be equalized to a desired target, $g(D)$, using an FIR filter, $f(D)$. Define $\varepsilon_i = z_i - d_i$ to be the difference between the equalized channel sample z_i and the desired target sample d_i at time index i. The 1-D equalizer with FIR $f(D)$ minimizes the mean-square error (MSE), $E\{\varepsilon_i^2\}$. If a target $g(D)$ has not been specified, the FIR filter $f(D)$ and

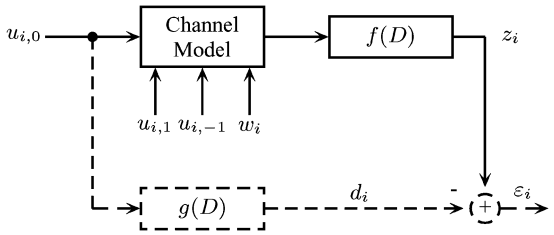

Fig. 6. 1-D MMSE equalizer design with FIR $f(D)$ and with a 1-D target $g(D)$ for BPM recording channels.

the target $g(D)$ are found simultaneously [14]. A 1-D MMSE FIR equalizer was also used in [7] where the FIR target was chosen to match the ISI of the main track.

Two-dimensional (2-D) equalization techniques have been used to shape 2-D channels such as holographic storage systems. The use of a 2-D GPR equalizer was proposed for BPM recording channels in [8] and [9]. Since this work is constrained to single track detection with single 1-D waveform obtained by a single read head, we only briefly review this 2-D equalization method that requires multiple 1-D waveforms as inputs.

In [8] and [9], the inputs to the 2-D equalizer were multiple 1-D waveforms which were obtained by reading multiple adjacent tracks. A monic constraint on the target response of the main track was imposed as well as an additional constraint that forces the ITI to zero. This method offered performance improvement compared to the 1-D equalization techniques described above. In [9], a simplified 2-D equalization technique produced the same results as in [8].

B. Joint-Track Equalization

In this study, we adapt the joint-track equalization technique introduced in [5] to BPM recording channels. The read channel model assumed is the same multi-input single-output system shown in Fig. 2. The joint-track equalization technique consists of a 1-D equalizer shown in Fig. 7(a). This 1-D equalizer not only equalizes the main track to a 1-D target but also equalizes all three tracks to a 2-D target as shown in Fig. 7(b). In contrast, the previously designed 1-D equalizers described in [13] and [7] only equalize the main track to a 1-D target.

In the joint-track equalization process, we design an MMSE equalizer with FIR $f(D) = \sum_{k=-\ell}^{\ell} f_k D^k$ using an adaptation of the method in [14] but with a 3×3 target response G

$$G = \begin{pmatrix} g_{0,-1} & g_{1,-1} & g_{2,-1} \\ g_{0,0} & g_{1,0} & g_{2,0} \\ g_{0,1} & g_{1,1} & g_{2,1} \end{pmatrix}. \tag{21}$$

Let

$$g_{-1}(D) = \sum_{k=0}^{2} g_{k,-1} D^k \tag{22}$$

$$g_0(D) = \sum_{k=0}^{2} g_{k,0} D^k \tag{23}$$

and

$$g_1(D) = \sum_{k=0}^{2} g_{k,1} D^k \tag{24}$$

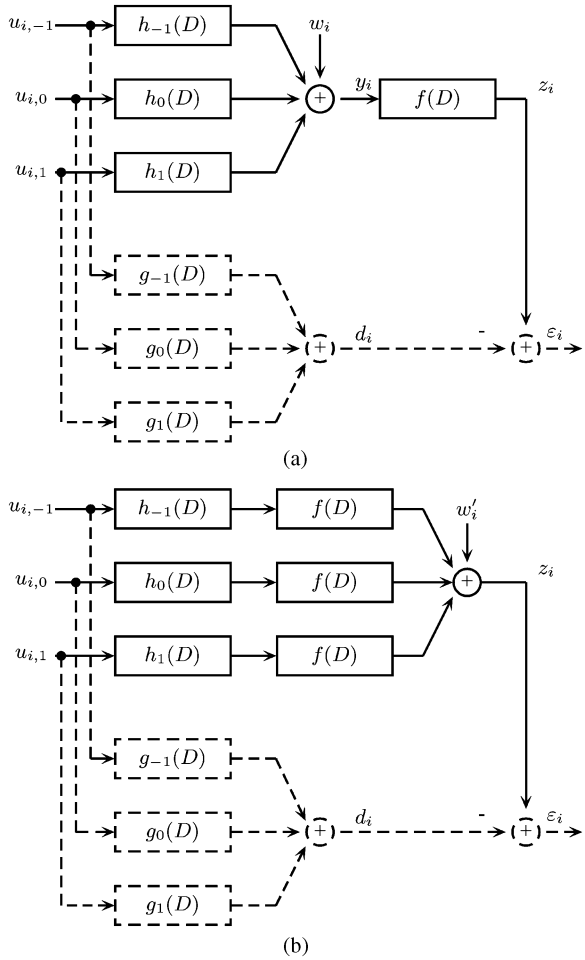

Fig. 7. (a) Block diagram for joint-track equalizer design. (b) Equivalent block diagram where w_i' represents the colored noise sample after equalization.

where $g_{-1}(D)$, $g_0(D)$, and $g_1(D)$ represent the targets for the upper, main, and lower track, respectively.

In [15], for a perpendicular magnetic recording channel with two interfering tracks, a joint-track equalizer with a monic constraint for the track to be detected was used. In contrast to the derivation in [15], by representing the 2-D data sequence and the 2-D target polynomial coefficients by vectors, the 2-D target design problem can be converted into a 1-D form. This method was used previously in [8], [16], and [9]. The joint-track equalizer can be obtained by setting the number of read heads to 1 and modifying the constraint matrix to incorporate the constraints on the target G in the equalization design of [8] and [9].

V. Simulation Results

In this section, we compare the performance and the complexity of several different schemes for recording densities of 1, 1.2, 1.4, 1.7, 1.75, and 2 Tb/in^2. We utilize a medium employing an SUL [2] with the media configurations shown in Table I. For a recording density of 1 Tb/in^2, the extent of ISI is limited to two symbols. For higher recording densities, the extent of ISI becomes four symbols due to the decreasing island separation distance in the down-track direction.

A. *Recording Density of 1 Tb/in^2*

For a recording density of 1 Tb/in^2, we utilize two different channel responses H_1 and H_2. Channel H_1 is obtained by a medium with no SUL [7] whereas channel H_2 is obtained by a medium employing an SUL [2]

$$H_1 = \begin{pmatrix} -0.023 & 0.264 & -0.023 \\ -0.087 & 1 & -0.087 \\ -0.023 & 0.264 & -0.023 \end{pmatrix} \quad (25)$$

$$H_2 = \begin{pmatrix} 0.0347 & 0.2297 & 0.0347 \\ 0.1277 & 1 & 0.1277 \\ 0.0347 & 0.2297 & 0.0347 \end{pmatrix}. \quad (26)$$

The negative entries in (25) are due to the assumption of no SUL.

For channels H_1 and H_2, we compare five different schemes. The first scheme utilizes an optimal bit detector, i.e., MAP bit detector. This scheme uses a reduced-state trellis with 36 states and eight outgoing branches per state as described Section II. The second scheme was introduced by Nabavi *et al.* [7]. Their scheme consists of a 1-D MMSE FIR equalizer with a PR target that closely matches the channel response of the main track. They represented their detector with a modified trellis that has four states with three parallel branches between each pair of connected states. Note that for the modified trellis, only the ITI from immediately adjacent bits are taken into account. The Viterbi algorithm with the squared-Euclidean metric is utilized to detect the symbol sequence. Since the detection of the main track sequence is considered, the detected bits belonging to the outer tracks obtained from the survivor branch out of the parallel branches are discarded. For channels H_1 and H_2, PR targets $[-0.1, 1, -0.1]$ and $[0.1, 1, 0.1]$ are chosen, respectively.

Simulation results for these two schemes are shown in Figs. 8 and 9. The numerical results for the second scheme were taken from [7] for channel H_1. The SNR is defined as follows:

$$\text{SNR} = 10 \log_{10} \left(\frac{V_p^2}{\sigma^2} \right) \quad (27)$$

where V_p is the peak value of the readback signal of an isolated island and σ^2 is the variance of the noise. Here, $V_p = 1$.

It can be seen from Figs. 8 and 9 that at a target bit error rate of 10^{-4}, for channels H_1 and H_2, the scheme that utilizes optimal bit detection provides gains of 1.5 dB and 0.6 dB as compared to the scheme that utilizes 1-D equalization with the specified PR targets, respectively. For channels H_1 and H_2, simulation results not shown here indicate that the scheme that utilizes an ML symbol sequence detector and outputs the middle bit of each detected symbol gives similar bit error rates compared to the scheme utilizing optimal bit detection.

We propose another scheme that utilizes joint-track equalization technique described in Section IV-B. For certain head and media configurations, the contribution of the corner entries to the readback signal is close to zero. Therefore, our target is a 3×3 matrix G defined in (21) with the corner entries $g_{0,-1}$, $g_{0,1}$, $g_{2,-1}$, and $g_{2,1}$ set equal to zero and the middle entry $g_{1,0}$ set equal to 1. The detector trellis has four states with four parallel branches between each connected pair of states as shown in Section III-A. We use the Viterbi algorithm with the squared-Euclidean metric to detect the symbol sequence. The detector then outputs the middle bit of each detected symbol in this sequence. Since the equalizer colors the electronics noise,

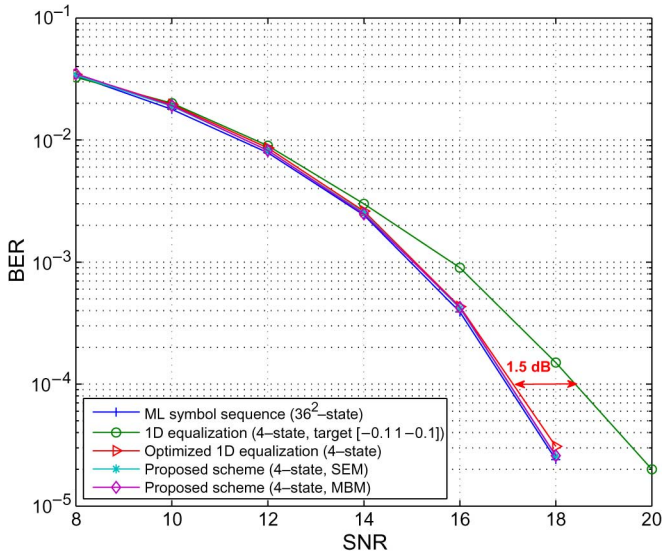

Fig. 8. Simulation results for channel H_1 (no SUL, 1 Tb/in^2). The acronyms SEM and MBM denote the squared-Euclidean metric and the modified branch metric, respectively.

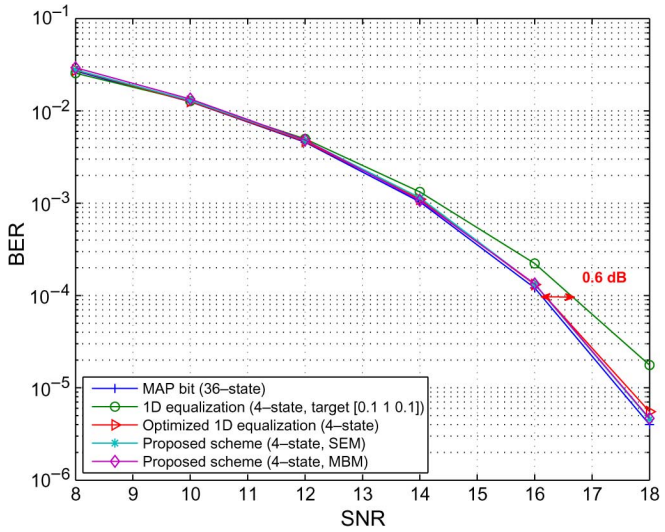

Fig. 9. Simulation results for channel H_2 (SUL, 1 Tb/in^2).

this detector is no longer ML. Note that the difference between the proposed scheme with the squared-Euclidean metric and the scheme described in [7] is the equalization methods utilized. However, both schemes have the same detection method. We also utilize the Viterbi algorithm with the modified branch metric defined by (18). This detector also does not output the ML bit sequence due to the noise coloration. For the performance curves, we utilize the acronyms SEM and MBM for the squared-Euclidean metric and the modified branch metric, respectively. Simulation results indicate that the proposed scheme with the squared-Euclidean metric or with the modified branch metric give virtually the same results. Note that computation of the modified branch metric is more complicated than computation of the squared-Euclidean metric.

We also consider the scheme in [7] with optimized 1-D equalizer/target coefficients. For this, different target choices are utilized. Simulation results show that the scheme in [7] has the best

performance when 1-D equalizer and target coefficients are obtained simultaneously in the MSE minimization process.

In all equalized systems, the FIR filters are limited to 11 taps. Simulation results in Figs. 8 and 9 show that the proposed scheme with joint-track equalization and the scheme with optimized 1-D equalizer/target coefficients essentially have the same performance as the scheme utilizing optimal bit detection.

B. Higher Recording Densities

For recording densities of 1.2 Tb/in^2, 1.4 Tb/in^2, 1.75 Tb/in^2, and 2 Tb/in^2, we have the following channel responses, respectively:

$$H_3 = \begin{pmatrix} 0 & 0.0572 & 0.2295 & 0.0572 & 0 \\ 0.003 & 0.2232 & 1 & 0.2232 & 0.003 \\ 0 & 0.0572 & 0.2295 & 0.0572 & 0 \end{pmatrix} \quad (28)$$

$$H_4 = \begin{pmatrix} 0.0035 & 0.0835 & 0.2294 & 0.0835 & 0.0035 \\ 0.01 & 0.3393 & 1 & 0.3393 & 0.01 \\ 0.0035 & 0.0835 & 0.2294 & 0.0835 & 0.0035 \end{pmatrix} \quad (29)$$

$$H_5 = \begin{pmatrix} 0.0136 & 0.1211 & 0.2293 & 0.1211 & 0.0136 \\ 0.0426 & 0.5080 & 1 & 0.5080 & 0.0426 \\ 0.0136 & 0.1211 & 0.2293 & 0.1211 & 0.0136 \end{pmatrix} \quad (30)$$

and

$$H_6 = \begin{pmatrix} 0.0257 & 0.1402 & 0.2292 & 0.1402 & 0.0257 \\ 0.0886 & 0.5937 & 1 & 0.5937 & 0.0886 \\ 0.0257 & 0.1402 & 0.2292 & 0.1402 & 0.0257 \end{pmatrix}. \quad (31)$$

These channels have memory of four symbols, so the scheme that utilizes optimal bit detection or ML symbol sequence detection utilize a reduced-state trellis with $6^4 = 36^2$ states. The computational complexity for optimal bit detection is very high. Therefore, we utilize only the ML symbol sequence detector that outputs the middle bit of each detected symbol. Note that this scheme can be viewed as a high SNR approximation for ML bit sequence detection as discussed in Section III-A.

In all equalized systems, the target length is limited to 3. For channel H_3, we choose a PR target [0.2, 1, 0.2] that closely matches to the channel response of the main track. In channels H_4, H_5, and H_6, in addition to the ITI from immediately adjacent bits on the outer tracks, the ITI from other bits is also significant. The performance curves not shown here indicate that the scheme using 1-D equalization with a PR target has poor performance for channels H_4, H_5, and H_6.

Simulation results for channel H_3 are shown in Fig. 10. It is seen that the scheme that utilizes ML symbol sequence detection offers 1.8 dB gain compared to the scheme that utilizes 1-D equalization with the PR target [0.2, 1, 0.2]. Simulation results also show that the proposed scheme with joint-track equalization and the scheme with optimized 1-D equalizer/target coefficients have the same performance as the scheme utilizing ML symbol sequence detection.

Simulation results are shown in Figs. 11, 12, and 13 for channels H_4, H_5, and H_6, respectively. For channels H_4 and H_5, the scheme that utilizes ML symbol sequence detection offers 0.5 dB and 5 dB gain as compared to the proposed scheme with joint-track equalization at a target bit error rate of 10^{-4}. For channels H_5 and H_6, the proposed scheme with joint-track equalization performs poorly as compared to the scheme that utilizes ML symbol sequence detection. This is due to severe noise coloration. This suggests choosing targets,

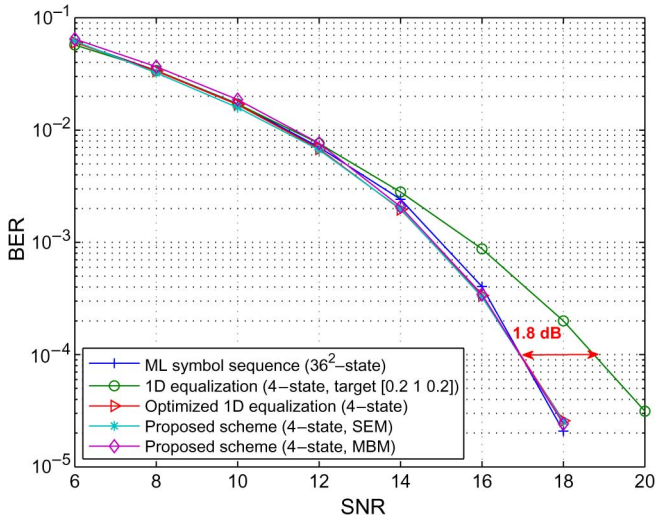

Fig. 10. Simulation results for channel H_3 (SUL, 1.2 Tb/in^2).

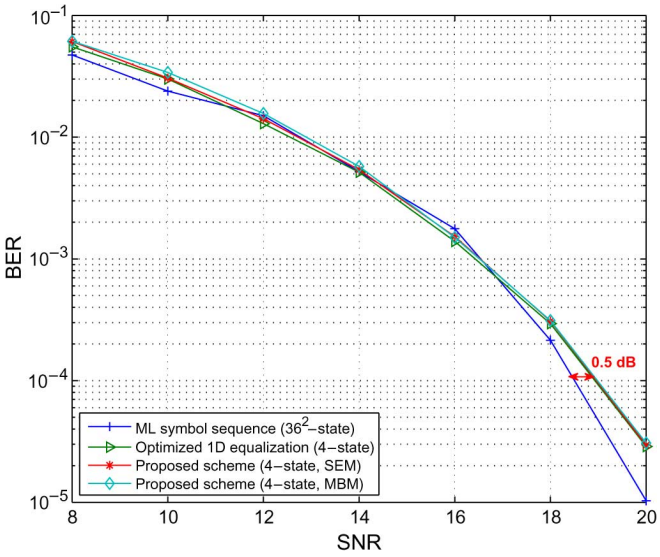

Fig. 11. Simulation results for channel H_4 (SUL, 1.4 Tb/in^2).

such as a longer target, which introduce less noise coloration or a noise whitening process before detection.

Simulation results show that for the channels considered above, the proposed scheme with joint-track equalization does not provide any gain compared to the scheme with optimized 1-D equalizer/target coefficients. We observe that the channels considered above have similar levels of ITI. Therefore, we study channels which have higher levels of ITI compared to the channels above. For this, consider channels H_7 and H_8

$$H_7 = \begin{pmatrix} 0.0037 & 0.1232 & 0.3813 & 0.1232 & 0.0037 \\ 0.0079 & 0.3133 & 1 & 0.3133 & 0.0079 \\ 0.0037 & 0.1232 & 0.3813 & 0.1232 & 0.0037 \end{pmatrix} \quad (32)$$

$$H_8 = \begin{pmatrix} 0.0038 & 0.1322 & 0.4118 & 0.1322 & 0.0038 \\ 0.0079 & 0.3135 & 1 & 0.3135 & 0.0079 \\ 0.0038 & 0.1322 & 0.4118 & 0.1322 & 0.0038 \end{pmatrix}. \quad (33)$$

Channels H_7 and H_8 are obtained for the media configurations where $s_x = 9$ nm, $s_z = 11$ nm, $B_x = 19$ nm, and $B_z = 22$ nm corresponding to 1.7 Tb/in^2. The MR head with the same

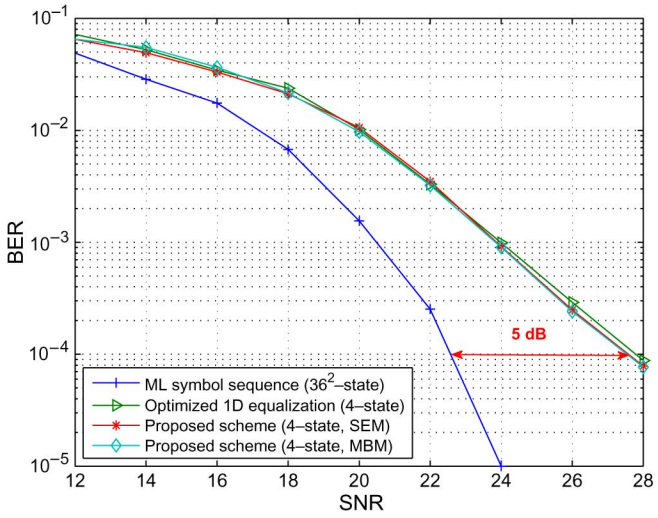

Fig. 12. Simulation results for channel H_5 (SUL, 1.75 Tb/in^2).

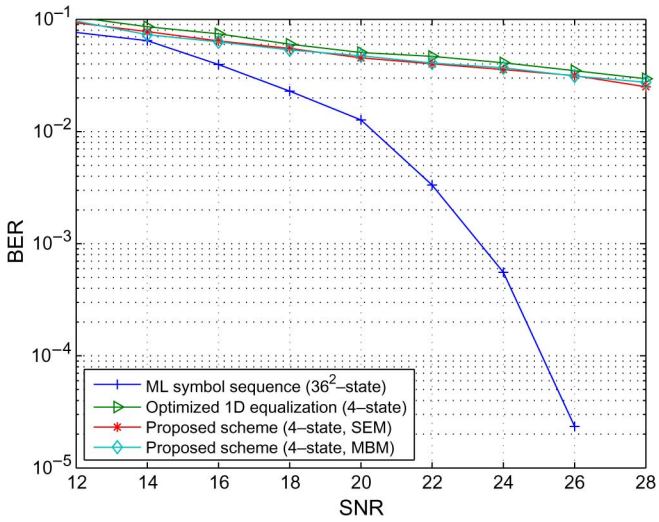

Fig. 13. Simulation results for channel H_6 (SUL, 2 Tb/in^2).

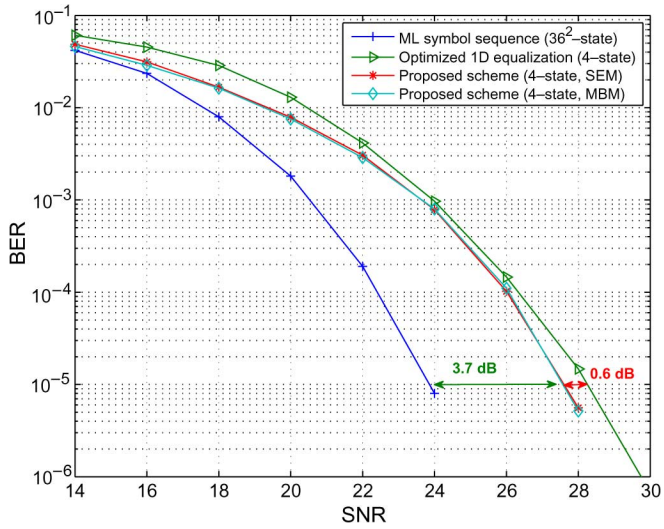

Fig. 14. Simulation results for channel H_7 (SUL, 1.7 Tb/in^2).

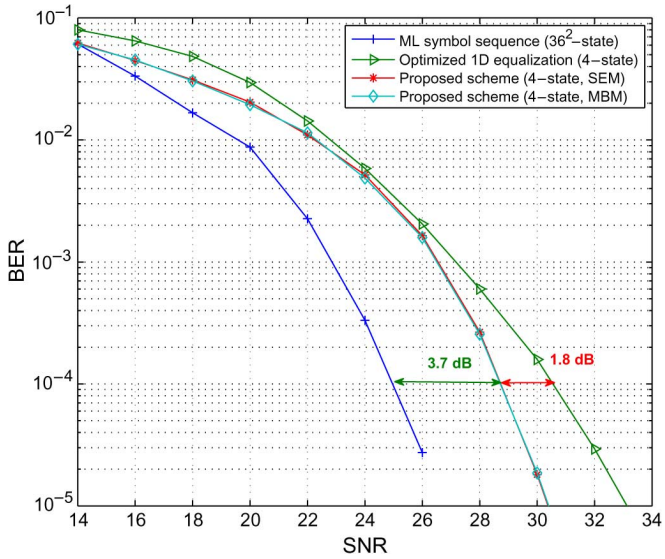

Fig. 15. Simulation results for channel H_8 (SUL, 1.7 Tb/in^2).

parameters described in Section II is utilized for channel H_7 whereas only the width of the MR element is raised to 41 nm from 40 nm for channel H_8.

For channel H_7, BER curves in Fig. 14 show that there is performance difference which is 0.6 dB at a target BER 10^{-5} between the proposed scheme with joint-track equalization and the scheme with optimized 1-D equalizer/target coefficients. However, for channel H_8, the proposed scheme with joint-track equalization outperforms the scheme with optimized 1-D equalizer/target coefficients with 1.8 dB at a target BER 10^{-4} as shown in Fig. 15. Note also that the scheme that outputs the middle bit sequence in the ML symbol sequence outperforms the proposed scheme with joint-track equalization with close to 3.7 dB difference at a target BER 10^{-5} and BER 10^{-4} for channels H_7 and H_8, respectively. This is an expected result since equalization introduces noise coloration which is not taken into account in the detection process.

Note that 2-D equalization techniques that eliminate the ITI as described in [8] and [9] would offer performance improvement compared to the schemes as described above. Nevertheless, as inputs, multiple 1-D waveforms rather than a single 1-D waveform are required for 2-D equalization.

C. Computational Complexity

Here, we compare the detection complexity of the schemes discussed above. The branch metric computations for the modified BCJR algorithm are more complex than the branch metric computations for the Viterbi algorithm. Therefore, the computational complexity of the scheme that utilizes the modified BCJR algorithm for optimal bit detection is substantially higher than the scheme that utilizes the Viterbi algorithm if both schemes work on the same detection trellis. For the recording density of 1 Tb/in^2, the scheme that utilizes optimal bit detection and the scheme that utilizes ML symbol sequence detection that outputs the middle bit in each detected symbol work on the same 36-state trellis. Hence, the latter scheme has less computational complexity.

The schemes that utilize a fixed PR target or optimized 1-D equalizer/target coefficients, and the proposed scheme with

joint-track equalization and the squared-Euclidean metric work on a 4-state trellis. It is seen that these schemes have the same total number of branches between all connected pairs of states when the branches between each connected pair of states that have the same noiseless channel outputs are merged. Therefore, they require the same computational complexity for the branch metric calculations between all pairs of connected states. In these schemes, one comparison is made to select one branch that accumulates the largest branch metric among parallel branches between each pair of connected states. The branch metric of the selected branch is added to the metric of the state from which the selected branch stems. Then, among the paths starting at different states, the path with the largest accumulated metric is selected for every state. Note that the proposed scheme with joint-track equalization and the squared-Euclidean metric and the schemes that utilize a fixed PR target or optimized 1-D equalizer/target coefficients require the same number of arithmetic operations. Therefore these schemes have the same computational complexity.

The scheme that utilizes ML symbol sequence detection that outputs the middle bit in each detected symbol works on the 36-state trellis or on the 36^2-state trellis depending on the recording density. This scheme requires a substantially higher number of arithmetic operations compared to the schemes that utilize a 4-state trellis, namely the proposed scheme with joint-track equalization and the schemes that utilize a fixed PR target or optimized 1-D equalizer/target coefficients. Thus, the scheme that utilizes ML symbol sequence detection that outputs the middle bit in each detected symbol has higher computational complexity compared to the proposed scheme with joint-track equalization and the schemes that utilize a fixed PR target or optimized 1-D equalizer/target coefficients.

The proposed scheme with joint-track equalization and the modified branch metric also works on a 4-state trellis. Note that the proposed scheme with joint-track equalization and the modified branch metric has less total number of branches between all pairs of connected states than the proposed scheme with joint-track equalization and the squared-Euclidean metric and the schemes that utilize a fixed PR target or optimized 1-D equalizer/target coefficients. However, the proposed scheme with joint-track equalization and the modified branch metric requires more arithmetic operations for the total number of branch metric calculations. Overall, it has higher computational complexity compared to the proposed scheme with joint-track equalization and the squared-Euclidean metric and the schemes that utilize a fixed PR target or with optimized 1-D equalizer/target coefficients.

VI. Conclusion

We considered a joint-track equalization procedure and compared several different detection and equalization methods for bit patterned media (BPM) recording channels. For the special case of a symmetric channel response matrix, we presented a maximum-likelihood (ML) bit sequence detector using the Viterbi algorithm with the modified branch metric. We proposed a scheme that utilizes the joint-track equalization technique followed by the Viterbi detector. The proposed scheme with a 3×3 target choice where the corner entries set equal to zero and the middle entry set equal to 1 outperforms the scheme of the same complexity that utilizes one-dimensional (1-D) equalization with a fixed partial-response (PR) target [7]. The performance of the proposed scheme with joint-track equalization and the scheme with optimized 1-D equalizer/target coefficients is comparable to that of the much more complex schemes utilizing optimal bit detection or optimal symbol sequence detection for recording densities of 1 Tb/in^2 and 1.2 Tb/in^2. However, the proposed scheme with joint-track equalization performs significantly better compared to the scheme with optimized 1-D equalizer/target coefficients in the presence of high level of inter-track interference (ITI). With increasing recording densities, the performance gap between the scheme that utilizes optimal symbol sequence detection and the schemes with equalization increases due to the noise coloration after equalization. Therefore, a noise whitening process or targets that introduce less noise coloration before detection are required.

Acknowledgment

This work was supported by the Patterned Media Project at Center for Magnetic Recording Research, University of California, San Diego.

References

[1] G. F. Hughes, "Patterned media recording systems—The potential and the problems," in *Intermag Dig. Tech. Papers*, Apr. 2002, p. GA6.

[2] S. Karakulak, P. H. Siegel, J. K. Wolf, and H. N. Bertram, "A new read channel model for patterned media storage," *IEEE Trans. Magn.*, vol. 44, no. 1, pp. 193–197, Jan. 2008.

[3] H. Burkhardt, "Optimal data retrieval for high density storage," in *Proc. CompEuro '89., VLSI and Computer Peripherals. VLSI and Microelectronic Applications in Intelligent Peripherals and Their Interconnection Networks*, May 1989, pp. 43–48.

[4] J. F. Heanue, K. Gurkan, and L. Hesselink, "Signal detection for page-access optical memories with intersymbol interference," *Appl. Opt.*, pp. 2341–2348, May 1996.

[5] B. G. Roh, S. U. Lee, J. Moon, and Y. Chen, "Single-head/single-track detection in interfering tracks," *IEEE Trans. Magn.*, vol. 38, no. 4, pp. 1830–1838, Jul. 2002.

[6] W. Tan and J. R. Cruz, "Evaluation of detection algorithms for perpendicular recording channels with intertrack interference," *J. Magn. Magn. Mater.*, vol. 287, pp. 397–404, 2005.

[7] S. Nabavi, B. V. K. V. Kumar, and J.-G. Zhu, "Modifying Viterbi algorithm to mitigate inter-track interference in bit-patterned media," *IEEE Trans. Magn.*, vol. 43, no. 6, pp. 2274–2276, Jun. 2007.

[8] S. Nabavi and B. V. K. V. Kumar, "Two-dimensional generalized partial response equalizer for bit-patterned media," in *Proc. IEEE International Conf. on Communications (ICC'07)*, Jun. 2007, pp. 6249–6254.

[9] M. Keskinoz, "Two-dimensional equalization/detection for patterned media storage," *IEEE Trans. Magn.*, vol. 44, no. 4, pp. 533–539, Apr. 2008.

[10] S. W. Yuan and H. N. Bertram, "Off-track spacing loss of shielded MR heads," *IEEE Trans. Magn.*, vol. 30, no. 3, pp. 1267–1273, May 1994.

[11] S. W. Yuan and H. N. Bertram, "Correction to "Off-track spacing loss of shielded MR heads"," *IEEE Trans. Magn.*, vol. 32, no. 4, p. 3334, Jul. 1996.

[12] L. Bahl, J. Cocke, F. Jelinek, and J. Raviv, "Optimal decoding of linear codes for minimizing symbol error rate," *IEEE Trans. Inform. Theory*, vol. IT-20, pp. 284–287, Mar. 1974.

[13] P. W. Nutter, I. T. Ntokas, and B. K. Middleton, "An investigation of the effects of media characteristics on read channel performance for patterned media storage," *IEEE Trans. Magn.*, vol. 41, no. 11, pp. 4327–4334, Nov. 2005.

[14] J. Moon and W. Zeng, "Equalization for maximum likelihood detectors," *IEEE Trans. Magn.*, vol. 31, no. 2, pp. 1083–1088, Mar. 1995.

[15] W. Tan and J. R. Cruz, "Signal processing for perpendicular recording channels with intertrack interference," *IEEE Trans. Magn.*, vol. 41, no. 2, pp. 730–735, Feb. 2005.

[16] L. Huang, G. Mathew, and T. C. Chong, "Channel modeling and target design for two-dimensional optical storage systems," *IEEE Trans. Magn.*, vol. 41, no. 8, pp. 2414–2424, Aug. 2005.